

Ligand Substitution, Catalyst Activation, and Oxidative Addition Studies of a Stable Dialkyl Palladium Precatalyst

Ian C. Chagunda, Antonia Kropp, David C. Leitch,* and J. Scott McIndoe*

Cite This: *Organometallics* 2025, 44, 628–636

Read Online

ACCESS |



Metrics & More

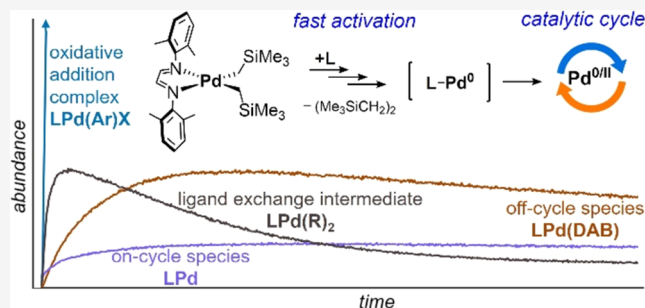


Article Recommendations



Supporting Information

ABSTRACT: Palladium-catalyzed cross-coupling reactions are indispensable in chemical synthesis, but efficient *in situ* catalyst activation remains a persistent challenge. Current Pd(II) precatalysts often lead to inefficient catalyst activation, necessitating higher catalyst loadings and limiting selectivity. We investigated the ligand substitution and activation mechanism of the stable Pd(II) dialkyl complex (^{DMP}DAB)Pd(CH₂SiMe₃)₂ in real-time using mass spectrometric monitoring. The introduction of charge-tagged phosphine ligands enabled the detection of key catalytic intermediates and identification of off-cycle species. Our findings demonstrate a low activation energy for the ligand dissociation of the ^{DMP}DAB ligand and the reductive elimination of (Me₃SiCH₂)₂ resulting in rapid formation of monoligated LPd(0) species, the active catalytic species for oxidative addition. These mechanistic insights offer a path toward developing more efficient and selective Pd-catalyzed processes, offering valuable guidance for the future design of precatalysts with improved performance.



INTRODUCTION

Palladium-catalyzed cross-coupling is a significant tool in modern chemical synthesis, with its development, scope, and limitations having been reviewed extensively.^{1–5} The widely accepted mechanism of cross-coupling reactions comprises three basic steps: oxidative addition, transmetalation, and reductive elimination, with a catalyst activation step often preceding oxidative addition to generate the active catalytic species from the precatalyst.

The nature of the active species in the catalytic cycle is one of the main issues in cross-coupling reactions. Precursors like Pd₂(dba)₃·solvent,^{6,7} [Pd(allyl)Cl]₂, and Pd(OAc)₂⁸ have typically been used with appropriate ligands to produce the active Pd(0) complexes *in situ* (Figure 1A); however, the formation of a specific active catalytic species can be challenging to achieve when using *in situ* catalysis.⁹ This method may lead to catalytic processes that are not as efficient overall in terms of catalyst loading, conversion, and selectivity, owing to unwanted off-cycle reaction pathways.^{10,11}

While L_nPd(0) complexes are widely recognized as the active catalytic species, the exact ligation state—monoligated (*n* = 1), bisligated (*n* = 2), or both—remains unclear in many cases.¹¹ Monoligated LPd(0) complexes are sufficiently reactive that they have not been isolated,^{12,13} whereas many examples of bisligated L₂Pd(0) complexes are commercially available.^{14,15} Notably the catalytic activity of monoligated and bisligated complexes can significantly differ, even with the same ligand used.¹⁶ Factors such as ligand size and ligand-to-precatalyst molar ratio play a crucial role in determining the preference for mono- or bisligation.^{17–19} Crucially, the ligation

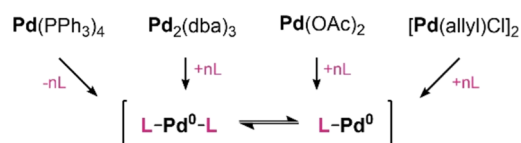
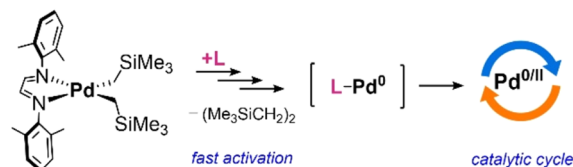
A Common Pd sources for *in situ* LnPd(0) catalyst formationB Pd(II) precatalyst for *in situ* LPd(0) catalyst formation

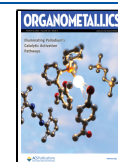
Figure 1. (A) Common Pd(II) and Pd(0) sources for *in situ* LnPd(0) catalyst formation, where controlling the ligation state can be challenging. (B) New dialkyl Pd(II) precatalyst (^{DMP}DAB)Pd(CH₂SiMe₃)₂ for controlled *in situ* LPd(0) generation without the need for preinstallation of ligand L.

Received: October 30, 2024

Revised: December 16, 2024

Accepted: December 30, 2024

Published: January 6, 2025



state also influences the mechanistic pathways for oxidative addition, where $\text{LPd}(0)$ tends toward a 3-centered concerted mechanism, while $\text{L}_2\text{Pd}(0)$ complexes can favor a nucleophilic displacement mechanism. This mechanistic divergence can lead to differential site-selectivity preferences in certain cases.^{20–23}

Recently, the activation of appropriate precatalysts has made it possible to generate highly reactive $\text{LPd}(0)$ species under controlled reaction conditions thanks to advancements in ligand and catalyst design.^{24–36} Many of these new-generation precatalysts exist as preligated $\text{Pd}(\text{II})$ complexes that are air- and moisture-stable, and rapidly activate under the reaction conditions. This leads to high reactivity with lower catalyst loadings, enabling expanded applicability and selectivity.³⁷ In parallel, preligated $\text{Pd}(0)$ precatalysts bearing throw-away ligands such as cyclopentadiene (COD), divinyl-disiloxanes (dvds), or maleic anhydride have also been developed.^{38–43} These ligands serve as sacrificial components, stabilizing the $\text{Pd}(0)$ species during handling while dissociating readily under reaction conditions, offering another route to accessing reactive $\text{LPd}(0)$ species. However, these precatalysts all require preinstallation of the ancillary ligand L , and options for *in situ* ligation/activation are still limited.

A recent solution to these issues is the $\text{Pd}(\text{II})$ dialkyl complex $(^{\text{DMP}}\text{DAB})\text{Pd}(\text{CH}_2\text{SiMe}_3)_2$ ($^{\text{DMP}}\text{DAB} = N,N'$ -bis(2,6-dimethylphenyl)diazabutadiene, Figure 1B).⁴⁴ This precatalyst does not require the preinstallation of ancillary ligands, potentially enabling greater versatility in a broader range of reaction conditions. It has shown high activity for *in situ* catalyst formation in challenging Suzuki and Heck reactions. It is also an ideal precursor to generate isolable oxidative addition complexes (OACs), a class of complexes relevant to both mechanistic studies and late-stage functionalization of pharmaceutical scaffolds.^{28,44,45} Additionally, its thermal and air stability and high solubility in many organic solvents make $(^{\text{DMP}}\text{DAB})\text{Pd}(\text{CH}_2\text{SiMe}_3)_2$ a versatile Pd source for high-throughput experimentation.

Herein we report a mechanistic examination of catalyst activation for $(^{\text{DMP}}\text{DAB})\text{Pd}(\text{CH}_2\text{SiMe}_3)_2$ using charge-tagged phosphine ligands, and the ensuing oxidative addition reaction with aryl halides (previously preprinted at ref 46). Using pressurized sample infusion-electrospray ionization-mass spectrometry (PSI-ESI-MS),⁴⁷ catalytic intermediates and off-cycle reaction pathways are studied in real-time. PSI-ESI-MS has been shown to be a valuable tool in studying catalytic reactions, with the use of charge-tagged ligands facilitating the detection of transient catalytic intermediates which can be challenging to identify using other techniques. Specifically, with *sSPhos*, we observe extremely rapid formation of $\text{LPd}(0)$ by ligand substitution and C–C reductive elimination, even at low concentration. We have also identified key intermediates and potential off-cycle species where the $^{\text{DMP}}\text{DAB}$ ligand remains coordinated to Pd . These insights lead to a more complete mechanistic picture of how $(^{\text{DMP}}\text{DAB})\text{Pd}(\text{CH}_2\text{SiMe}_3)_2$ operates when used as a precursor for ArX oxidative addition or catalysis.

RESULTS AND DISCUSSION

Investigation of Catalyst Activation Processes. Mono-ligated $\text{LPd}(0)$ species have been described as difficult, if not impossible, to define clearly in solution.⁴⁸ While theoretical investigations have provided some insight into the energetics of such species,^{49–51} definitive solution phase detection

remains elusive due to their coordinatively unsaturated and consequently highly reactive nature. Advancements in this area has been made with identification by MS.^{16,52} However, using MS techniques to determine the solution phase structures does have limitations, particularly if the ionization process imparts enough internal energy to ions resulting in fragmentation of weakly coordinating ligands.^{53–55} A semisystemic optimization of instrument parameters was therefore conducted using OptiMS⁵⁶ to minimize ion fragmentation and mitigate the stated limitation in characterization by MS.

Initial investigations of the catalyst activation process were conducted using a charge-tagged phosphine $[(\text{Ph}_3\text{P})_2\text{N}]^+[\text{sSPhos}]^-$ (hereafter $[\text{PPN}][\mathbf{1}]$), obtained following a counterion exchange from the commercially available sulfonated dialkylbiaryl phosphine ligand $[\text{Na}]^+[\text{sSPhos}]^-$. Catalyst activation was initiated by introduction of a solution of precatalyst $(^{\text{DMP}}\text{DAB})\text{Pd}(\text{CH}_2\text{SiMe}_3)_2$ (tetrahydrofuran solvent) into a solution of $[\text{PPN}][\mathbf{1}]$ (methanol solvent) and monitoring the disappearance of $[\mathbf{1}]^-$ (m/z 498) and the appearance of catalyst activation species. The use of the charged ligand enabled observation of ordinarily neutral catalytic species that are otherwise unobservable by MS. Additionally, using charged ligands enabled operating the instruments at low source voltages, while maintaining strong signal intensities as previously demonstrated.^{10,57,58}

Several Pd -containing species were observed and identified by their m/z ratios; measured isotopic distribution patterns also match calculated patterns (see Supporting Information (SI), Table S3 and Figure S2). The primary species, generated immediately upon addition of $(^{\text{DMP}}\text{DAB})\text{Pd}(\text{CH}_2\text{SiMe}_3)_2$, is assigned as monoligated $[\text{Pd}(\mathbf{1})]^-$ (m/z 595) (Figure 2). The formation of $[\text{Pd}(\mathbf{1})]^-$ was evident within the time required to transfer the solution from the reaction flask to the spectrometer inlet (approximately 25 s),⁴⁷ suggesting a rapid initiation process. This species is formed by ligand exchange and C–C reductive elimination, both of which happen extremely rapidly even at low concentration (10 μM). The observed consumption of free ligand (Figure 2A) occurs over a longer time scale (approximately 5 min), indicating that ligand coordination and subsequent reduction likely proceed with a half-life closer to 60 s under the experimental conditions. No bisligated $[\text{Pd}(\mathbf{1})_2]^{2-}$ species were observed under these conditions, even when 2 equiv of $\mathbf{1}$ were added (see SI Figure S3); however, bisligation is evident with a larger excess of $\mathbf{1}$ (*vide infra*). Over time, we observe evidence of phosphine oxidation, a common deactivation pathway in palladium-catalyzed reactions.⁵⁹ The major Pd species observed is assigned as $[\text{Pd}(\mathbf{1}) + \text{O}]^-$ (m/z 611), which is generated alongside the phosphine oxide $[\mathbf{1} + \text{O}]^-$ (m/z 517). This deactivation of monoligated $[\text{Pd}(\mathbf{1})]^-$ is consistent with the highly reactive nature of this coordinatively unsaturated species.

Despite following best practices to maintain an anaerobic environment, minor air contamination can occur during the injection of solutions into reaction flasks. This air contamination, along with trace dissolved gases in the solvent, can lead to excessive observable oxidation side products, further accentuated by the extremely low operating concentrations used for ESI-MS experiments.⁴⁷ Consequently, the oxidation side products observed may be more prominent in these experiments than they would be under typical preparative-scale conditions.

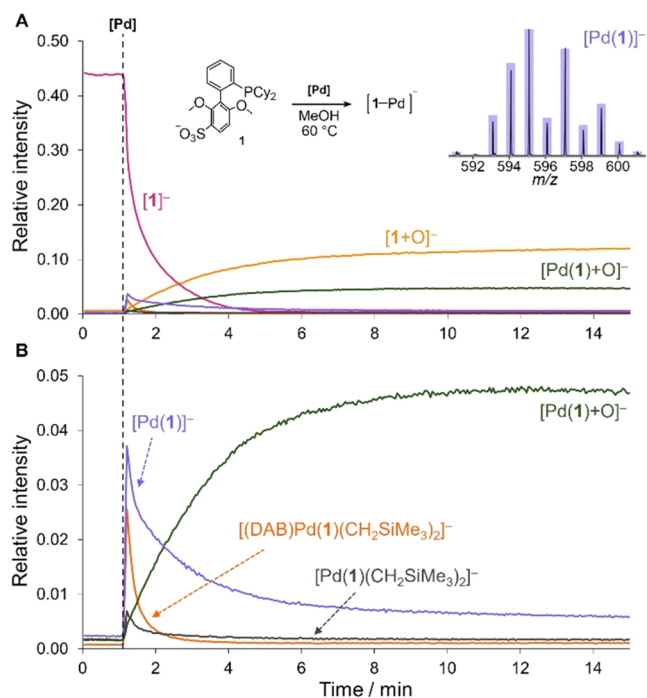


Figure 2. (A) PSI-ESI(-)-MS reaction monitoring of catalyst activation upon addition of $(\text{DMPDAB})\text{Pd}(\text{CH}_2\text{SiMe}_3)_2$ (10 μM , 1.0 equiv, at 1.0 min) to a solution of $[\text{PPN}][\mathbf{1}]$ (10 μM , 1.0 equiv) in MeOH, resulting in formation of $[\text{Pd}(\mathbf{1})]^-$, associative ligand exchange intermediates $[(\text{DMPDAB})\text{Pd}(\mathbf{1})(\text{CH}_2\text{SiMe}_3)_2]^-$ and $[\text{Pd}(\mathbf{1})(\text{CH}_2\text{SiMe}_3)_2]^-$, and ligand oxidation product $[\mathbf{1} + \text{O}]^-$. (B) Relative intensities axis amplified $\times 10$, highlighting key reaction intermediates. Inset: calculated isotopic distribution pattern (bars) overlaid on the experimental isotopic distribution (lines) for monoligated $[\text{Pd}(\mathbf{1})]^-$.

In addition to $[\text{Pd}(\mathbf{1})]^-$, we also detected two Pd(II) ligand exchange intermediates: $[(\text{DMPDAB})\text{Pd}(\mathbf{1})(\text{CH}_2\text{SiMe}_3)_2]^-$ (m/z 1033) and $[\text{Pd}(\mathbf{1})(\text{CH}_2\text{SiMe}_3)_2]^-$ (m/z 769). Further investigation focused on the intermediate $[(\text{DMPDAB})\text{Pd}(\mathbf{1})(\text{CH}_2\text{SiMe}_3)_2]^-$ using ESI-MS/MS techniques, where inducing the unimolecular decomposition provided a detailed picture of the fragmentation pathway. Under collision-induced dissociation (CID) conditions, the precursor ion fragmented into three product ions: (1) $[\text{Pd}(\mathbf{1})(\text{CH}_2\text{SiMe}_3)_2]^-$ through loss of DMPDAB via ligand dissociation, (2) $[\text{Pd}(\mathbf{1})]^-$ through loss of $(\text{Me}_3\text{SiCH}_2)_2$ by reductive elimination, and (3) free $[\mathbf{1}]^-$ from ligand dissociation of the phosphine (Figure 3A). Notably, even at a collision energy (CE) of 0 V (SI Figure S3), precursor ion fragmentation occurred, indicating a low activation energy for dissociation of this intermediate. While we cannot definitively assign this as 4- or 5-coordinate, a monodentate binding mode for DMPDAB is consistent with both the bonding preferences of d^8 Pd(II), and the facile ligand dissociation at 0 V. This 4-coordinate species likely arises from $\mathbf{1}$ displacing one of the imine arms. The relatively low intensity of product ion $[\text{Pd}(\mathbf{1})]^-$ at CE 0 V contrasts with its higher abundance observed in the MS scans (Figure 2). This indicates that the monoligated $[\text{Pd}(\mathbf{1})]^-$ catalyst activation species in Figure 2 is not solely a result of in-source fragmentation.

We applied a transfer collision energy ramp from 0 to 30 V (in 1 V increments) to $[(\text{DMPDAB})\text{Pd}(\mathbf{1})(\text{CH}_2\text{SiMe}_3)_2]^-$, revealing the energy-dependent changes in precursor and product ion intensities (Figure 3B). The results indicate that

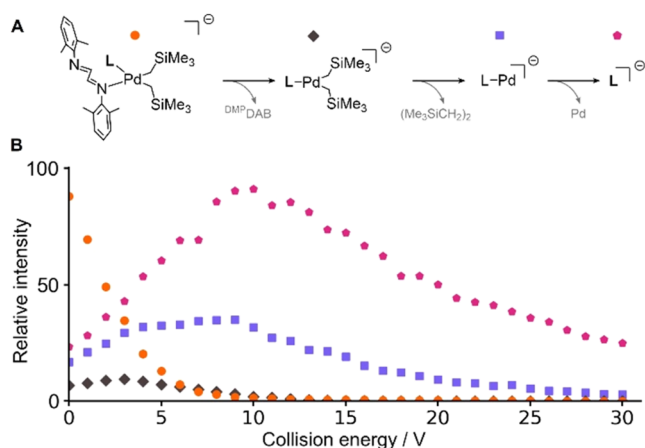


Figure 3. (A) Reaction pathway of $[(\text{DMPDAB})\text{Pd}(\mathbf{1})(\text{CH}_2\text{SiMe}_3)_2]^-$ ion fragmentation upon CID with argon gas, showing collision energies that maximized each product ion. Undetected neutral fragments shown in gray. (B) Relative intensities of precursor and product ions over a collision energy ramp (0–30, 1 V increments), highlighted with colors as in (A).

$[(\text{DMPDAB})\text{Pd}(\mathbf{1})(\text{CH}_2\text{SiMe}_3)_2]^-$ forms via a ligand association reaction, which undergoes further reactivity to generate the active catalyst. Initially, the precursor ion was at maximum intensity at CE 0 V and decreased rapidly as CE was increased. Notably, dissociation of DMPDAB is facile, as evidenced by the low activation energy required for fragmentation leading to $[\text{Pd}(\mathbf{1})(\text{CH}_2\text{SiMe}_3)_2]^-$. Subsequent reductive elimination of $(\text{Me}_3\text{SiCH}_2)_2$ generates the monoligated active catalyst $[\text{Pd}(\mathbf{1})]^-$, with the phosphine assisting the reductive elimination process through steric compression and transition state stabilization by coordination to the pendant arene.^{60–62} Crucially, the absence of a $[(\text{DMPDAB})\text{Pd}(\mathbf{1})]^-$ fragment ion indicates that the mechanistic steps follow a sequential pathway, as in Figure 3A, with DMPDAB ligand dissociation preceding the reductive elimination of $(\text{Me}_3\text{SiCH}_2)_2$. This observation aligns with literature studies demonstrating how reductive elimination in 4-coordinate d^8 complexes is often preceded by ligand dissociation, which generates a 3-coordinate intermediate.^{63,64} This reductive elimination is facilitated by the relative ease of polytopal rearrangement in this intermediate, enabling geometry distortion for advantageous orbital overlap.^{65–67}

In Situ Trapping of Monoligated $[\text{Pd}(\mathbf{1})]^-$. Once coordinatively unsaturated LPd(0) forms *in situ*, it should be susceptible to rapid trapping, either by ArX via oxidative addition, or alternatively through coordination with a stabilizing ligand such as an electron-deficient olefin.⁶⁸ We therefore sought to trap $[\text{Pd}(\mathbf{1})]^-$ in solution by adding an excess of the π -acidic ligand maleic anhydride (MAH). Our aim was to further evaluate whether $[\text{Pd}(\mathbf{1})]^-$ was a true solution phase species, rather than an in-source MS ion fragment of $[(\text{DMPDAB})\text{Pd}(\mathbf{1})(\text{CH}_2\text{SiMe}_3)_2]^-$ or of the bisligated $[\text{Pd}(\mathbf{1})_2]^{2-}$ species. Accordingly, after catalyst activation, we introduced 2 equiv of MAH to the reaction mixture (Figure 4). A sudden decrease in the signal intensity of $[\text{Pd}(\mathbf{1})]^-$ was observed, accompanied by a matching increase in the olefin-trapped Pd(0) species $[\text{Pd}(\mathbf{1})(\text{MAH})]^-$ (m/z 693). A much slower conversion between the two followed, which likely reflects the rate of reductive elimination of $(\text{Me}_3\text{SiCH}_2)_2$ from $[(\text{DMPDAB})\text{Pd}(\mathbf{1})(\text{CH}_2\text{SiMe}_3)_2]^-$ and/or

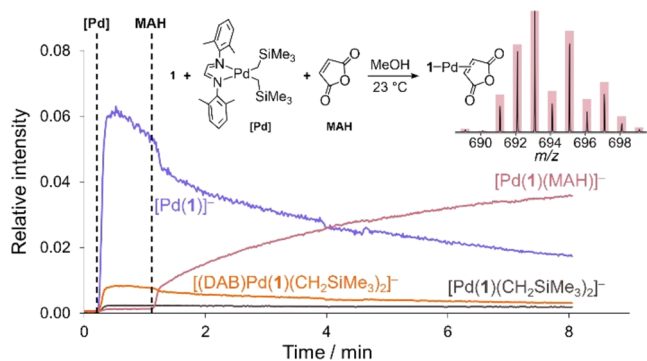


Figure 4. Relative species intensities for the introduction of maleic anhydride (MAH, 20 μM , 2 equiv, at 1.1 min) into a MeOH solution of [PPN][1] (10 μM , 1 equiv) and $(^{\text{DMP}}\text{DAB})\text{Pd}(\text{CH}_2\text{SiMe}_3)_2$ (10 μM , 1 equiv, at 0.1 min), monitored by PSI-ESI(-)-MS. MAH trapping yielded $[\text{Pd}(1)(\text{MAH})]^-$. Inset: calculated isotopic distribution patterns (bars) overlaid on the experimental isotopic distribution (lines) for $[\text{Pd}(1)(\text{MAH})]^-$.

the rate of bimolecular ligand association at these low concentrations.

Upon CID of $[\text{Pd}(1)(\text{MAH})]^-$ at CE 13 V, the primary fragment ion observed was $[\text{Pd}(1)]^-$ (see SI Figure S5). This trapping experiment further supports our assertion that $[\text{Pd}(1)]^-$ is indeed a solution-phase species, where the only other ligands are weakly bound and rapidly exchanging solvent molecules. This distinguishes it from a mere product of in-source ion fragmentation, where under these conditions (stoichiometric 1) the solution equilibrium strongly favors LPd(0) over $\text{L}_2\text{Pd}(0)$.

Ligand Competition Experiments. Previous studies have highlighted how ligand size influences the coordination number in $\text{L}_n\text{Pd}(0)$ species.^{18,20,62,69} We explored the impact different ligands have on catalyst activation through competitive experiments involving three phosphine ligands with varying sizes and denticity. To initiate catalyst activation, a precatalyst solution was introduced to a reaction flask containing equimolar amounts of charge-tagged phosphines sPhos (1), TPPMS (2), and ssXantphos (3). By maintaining a low precatalyst to ligand ratio (1:3 Pd/L), we aimed to observe preferential activation among these ligands.

Figure 5 shows the results of this experiment, with all three ligands exhibiting monoligated species upon activation. As a bidentate phosphine, 3 appears to form the more stable intermediate, although ion effects from the dianion likely result in suppression of the monoanionic intermediates. No homoleptic or heteroleptic bisligated species were observed for any of the ligands used in these experiments (see SI Figure S6). Additionally, all three ligands exhibited the associative ligand substitution intermediates $[(^{\text{DMP}}\text{DAB})\text{Pd}(\text{L})(\text{CH}_2\text{SiMe}_3)_2]^-$ and $[\text{Pd}(\text{L})(\text{CH}_2\text{SiMe}_3)_2]^-$ (see SI Table S3 and Figure S2), consistent with similar activation mechanisms. Notably, detection of $[\text{Pd}(3)(\text{CH}_2\text{SiMe}_3)_2]^-$ aligns favorably with previous work, where the analogous Pd(xantphos)- $(\text{CH}_2\text{SiMe}_3)_2$ complex was successfully isolated from $(^{\text{DMP}}\text{DAB})\text{Pd}(\text{CH}_2\text{SiMe}_3)_2$ in 68% yield.⁴⁴

The observed preference for monoligation under stoichiometric conditions implies an appreciable barrier to the formation of $\text{L}_2\text{Pd}(0)$ species. This is attributed to steric hindrance posed by bulky ligands, electrostatic repulsion of the anionic ligands, and the low concentration of these reaction mixtures. Additionally, dialkylbiaryl phosphine ligands exhibit

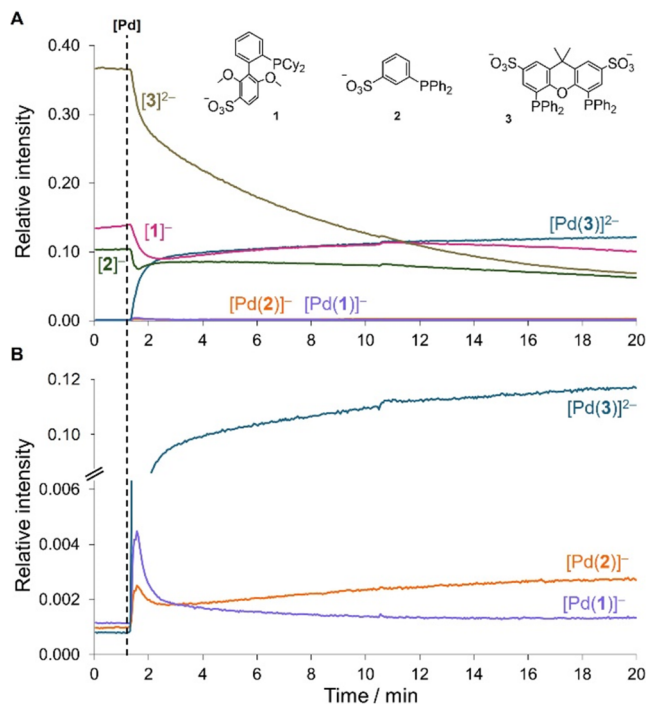


Figure 5. (A) PSI-ESI(-)-MS reaction monitoring of the addition of $(^{\text{DMP}}\text{DAB})\text{Pd}(\text{CH}_2\text{SiMe}_3)_2$ (2.5 μM , 1 equiv, at 1.5 min) into an equimolar MeOH solution at 40 $^\circ\text{C}$ containing [PPN][1] (2.5 μM , 1 equiv), [PPN][2] (2.5 μM , 1 equiv), and [PPN]₂[3] (2.5 μM , 1 equiv), showing relative rates of phosphine activation and formation of LPd(0) intermediates. (B) Relative intensities axis amplified $\times 5$ to highlight key reaction intermediates.

conformational flexibility and diverse binding modes. Among these, strong pendant arene-metal interactions effectively stabilize the metal in a bidentate manner. These interactions occur through coordination where the nonphosphine-containing ring of the biaryl framework can serve as a ligand for the Pd center *via* the *ipso* or *ortho* carbon, or alternatively through the 2-methoxy substituent for 1.^{28,61,70–72}

Despite the smaller size of phosphine 2, the formation of bisligated palladium species was unexpectedly elusive in initial stoichiometric trials. This outcome contradicts previous studies under similar conditions, where $\text{Pd}_2(\text{dba})_3$ was used as the palladium source, and bisligation of 2 was readily observed.^{73,74} To promote bisligation, we conducted control experiments by adding an excess of 2 (3:1 L/Pd molar ratio) to the reaction flask prior to introducing the precatalyst. Upon adding the precatalyst, $[\text{Pd}(2)_2]^{2-}$ was observed, with its relative abundance 1/5th that of $[\text{Pd}(2)]^-$ under these conditions (see SI Figure S7). Bisligation was also observed for 1 when using a 3:1 L/Pd molar ratio (see SI Figure S8). The relatively low ion fragmentation energy of $[\text{Pd}(1)_2]^{2-}$ at 7 V compared to $[\text{Pd}(1)]^-$ at 20 V further indicates unfavorable coordination of the second phosphine.

While this study provides valuable insights into the activation mechanisms of $(^{\text{DMP}}\text{DAB})\text{Pd}(\text{CH}_2\text{SiMe}_3)_2$ using phosphines 1, 2, and 3, these ligands primarily feature phenyl and secondary alkyl groups. The activation mechanism may differ when using bulkier phosphines such as PAD_3 , (*t*Bu)-XPhos, or (*t*Bu)BrettPhos which introduce greater steric hindrance. Further investigations are planned to explore the behavior of bulkier ligands, which will help elucidate the

generality of the observed activation pathways and provide a more comprehensive understanding of the system's behavior.

Oxidative Addition Reactivity. With the mechanisms of *in situ* catalyst activation to LPd(0) established, we next investigated the oxidative addition of this species with ArX. Initial investigations using the charge-tagged phosphine **1** yielded no detectable oxidative addition products by MS. Since oxidative addition complexes $L_nPd(Ar)(X)$ tend to produce cationic $[L_nPd(Ar)]^+$ species following halide dissociation in polar solvents under ESI-MS conditions,^{58,74–76} the charge-tagged analogue Pd(1)(Ar) would be zwitterionic and undetectable by MS. To address this, we switched to using the neutral dialkylbiaryl phosphine SPhos (**4**) and operated our MS instruments in positive ion mode, with **4** observed as the protonated species $[4+H]^+$ (m/z 411).

Investigation of the formation of OACs was achieved by introducing precatalyst into a solution containing **4** and an excess of 4'-bromoacetophenone (ArBr). Upon adding $(^{DMP}DAB)Pd(CH_2SiMe_3)_2$, the primary Pd(II) intermediate $[Pd(4)(Ar)]^+$ (m/z 635) formed rapidly through oxidative addition to ArBr (Figure 6A). After approximately 10 min, this

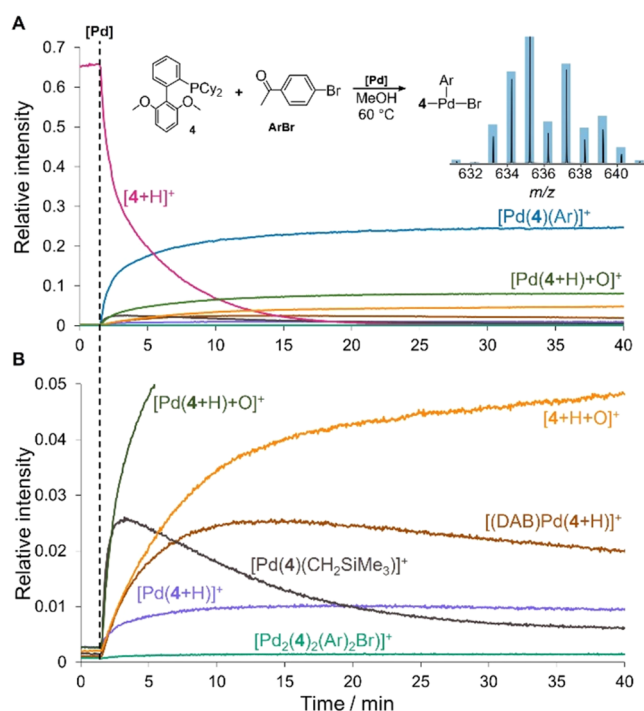


Figure 6. (A) PSI-ESI(+)-MS reaction monitoring of oxidative addition upon introduction of $(^{DMP}DAB)Pd(CH_2SiMe_3)_2$ (2.5 μ M, 1 equiv, at 1.0 min) into a MeOH solution containing **4** (2.5 μ M, 1 equiv) and ArBr (50 μ M, 20 equiv), forming $[Pd(4)(Ar)]^+$. (B) Key reaction intermediates and off-cycle products observed, with relative intensities axis amplified $\times 10$. Inset: calculated isotopic distribution patterns (bars) overlaid on the experimental isotopic distribution (lines) for $[Pd(4)(Ar)]^+$.

species reached a steady concentration. Analyzing the reaction intermediates (Figure 6B), we identified the ligand exchange intermediate $[Pd(4)(CH_2SiMe_3)]^+$ (m/z 603), which ionized *via* $[CH_2SiMe_3]^-$ loss, as the most abundant Pd-containing species immediately following precatalyst addition (see SI Figure S2 for isotopic distribution patterns for identified intermediates). As its abundance decreased, we also detected $[Pd(4+H)]^+$ (m/z 517), maintaining a steady concentration.

These sequential profiles lend support to the proposed ligand exchange and reductive elimination mechanism, consistent with the relative activation energies determined by CID (Figure 3).

Studies on Pd(L)(Ph)X OACs have highlighted their solvent-dependent behavior. Specifically, the halide-bridged dimeric form $[Pd(L)(Ph)(\mu-X)]_2$ tends to persist in non-coordinating solvents.⁷⁷ In our investigation, we detected evidence of dimer formation as the fragment ion $[Pd_2(4)_2(Ar)_2Br]^+$ (m/z 1351), which exhibited a kinetic profile similar to that of $[Pd(4)(Ar)]^+$. This equilibrium between dimers and monomers plays a crucial role, with dimer dissociation necessary for coordinating the nucleophilic coupling partner. Notably, we did not observe any $[(^{DMP}DAB)Pd(Ar)]^+$ species, which would result either from direct oxidative addition to a $(^{DMP}DAB)Pd(0)$ intermediate, or from ligand substitution between ^{DMP}DAB and $[Pd(4)(Ar)(Br)]$.

Beyond OAC formation, additional potential off-cycle reaction pathways and product formation was observed. Notably, palladium-catalyzed phosphine oxidation resulted in the formation of $[Pd(4+H)+O]^-$ (m/z 533) and $[(4+H+O)]^+$ (m/z 427), consistent with prior observations in the absence of ArX. Importantly, we detected the mixed ligand Pd(0) species $[(^{DMP}DAB)Pd(4+H)]^+$ (m/z 781), which also appeared in negative mode experiments as $[(^{DMP}DAB)Pd(1)]^-$ (m/z 861). This species likely arises from the coordination of free ^{DMP}DAB ligand to LPd(0). This means that ^{DMP}DAB could act as a catalyst inhibitor, maintaining a reservoir of less-reactive Pd(0). This behavior becomes evident when ArBr is sequentially added following catalyst activation (Figure 7).

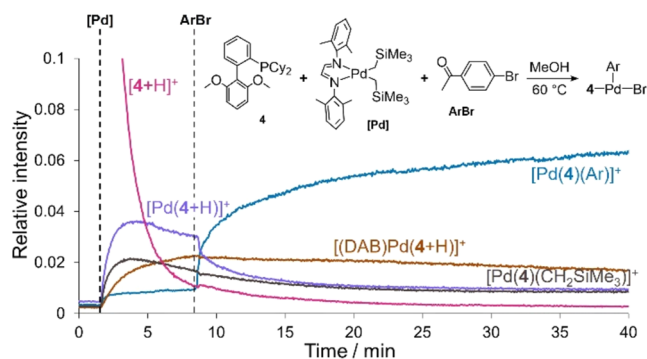


Figure 7. Relative species intensities for OAC formation by the sequential additions of $(^{DMP}DAB)Pd(CH_2SiMe_3)_2$ (2.5 μ M, 1 equiv, at 1.0 min) and ArBr (50 μ M, 20 equiv, at 8.0 min) into a MeOH solution containing **4** (2.5 μ M, 1.0 equiv). Experiment conducted under the same conditions as Figure 6, monitored by PSI-ESI(+)-MS.

Moreover, this sequential addition of precatalyst and ArBr further solidifies the role of monoligated $[Pd(4+H)]^+$ (m/z 517) as the active catalytic species, with its relative abundance decreasing in tandem with the formation of $[Pd(4)(Ar)]^+$.

Upon CID of $[Pd(4)(Ar)]^+$ at 32 V, multiple fragment ions emerged (Figure 8). Notably, one fragment ion, $[Pd(Ar')]^+$, was assigned to result from aryl exchange reactions between an aryl group originating from the Pd center (Ar) and another from the phosphine (Ar'). The aryl exchange reaction competes with the catalytic cycle, potentially contaminating the desired reaction product with products derived from the aryl group originally bound to the phosphorus. Generally, electron-rich aryl groups make exchange more facile, especially

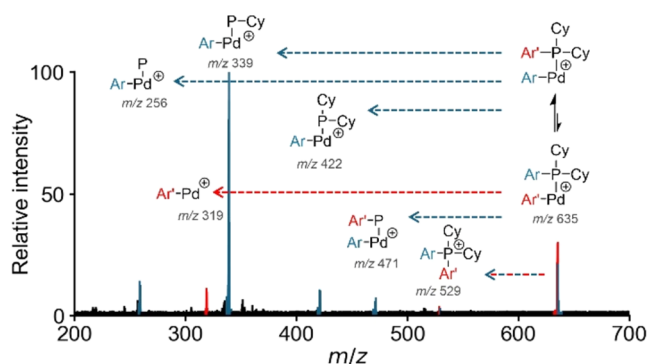


Figure 8. ESI(+)-MS/MS (CE = 32 V) of $[\text{Pd}(\mathbf{4})\text{Ar}]^+$ (m/z 635.4) showing product ions highlighted in blue, with product ion resulting from Pd-aryl/P-aryl exchange reaction $[\text{Pd}(\text{Ar}')]^+$ (m/z 319.1) highlighted in red. Key: Ar = $[\text{C}_6\text{H}_4\text{COCH}_3]$ originating from ArBr; Ar' = $[\text{C}_6\text{H}_4(\text{C}_6\text{H}_5(\text{OMe})_2)]$ originating from **4**.

in polar solvents and under dilute conditions.^{78–80} Additionally, trace amounts of the phosphonium salt $[\mathbf{4}\text{Ar}]^+$ (m/z 529), a proposed intermediate for aryl exchange, were generated through CID-induced reductive elimination of $[\text{Pd}(\mathbf{4})(\text{Ar})]^+$. In a test Suzuki cross-coupling reaction involving 4'-bromoacetophenone (ArBr) and 4-methoxyphenylboronic acid ($\text{RB}(\text{OH})_2$), we observed only trace contamination (<1%) from the aryl exchange product (see SI Figure S9). This observation is consistent with the aryl exchange rate being significantly lower than the rates of transmetalation and reductive elimination. Furthermore, the steric bulk of the ligand likely disfavors formation of the phosphonium salt intermediate in the solution phase.⁸¹ Nevertheless, this aryl transfer pathway is a potential source of both catalyst decomposition and product contamination, and should therefore be considered as a possible failure mode.

Proposed Catalytic Cycle. Drawing from our observations, we propose the following general reaction pathways for the *in situ* catalyst activation of $(^{\text{DMPDAB}}\text{Pd})(\text{CH}_2\text{SiMe}_3)_2$ to $\text{L}_n\text{Pd}(0)$ and the subsequent formation of OACs (Figure 9).⁸² The active Pd(0) species emerges through an associative ligand substitution, initially forming the 4-coordinate mixed ligand $(^{\text{DMPDAB}}\text{Pd})(\text{L})(\text{CH}_2\text{SiMe}_3)_2$, followed by dissociation of $^{\text{DMPDAB}}$. Subsequent reductive elimination of the two alkyl groups yields the monoligated $\text{LPd}(0)$, which remains stable due to interactions with ligand pendant arenes and/or coordinating solvent molecules. This highly active species then initiates the catalytic cycle for cross-coupling reactions, with the product of oxidative addition of ArX partially existing as monomeric $[\text{Pd}(\text{L})\text{Ar}]^+$ following halide loss in polar solvents under these ESI-MS conditions. Identified off-cycle pathways include phosphine oxidation if O_2 is present, as well as competitive inhibition by $^{\text{DMPDAB}}$. This latter aspect is an important consideration for achieving maximum catalytic rates, where a noninnocent $^{\text{DMPDAB}}$ “throw-away” ligand would impede catalytic turnover. Further studies to probe this reactivity under different catalytic conditions are underway.

CONCLUSIONS

In this study, we have established evidence for the activation mechanisms of the dialkyl-palladium precatalyst $(^{\text{DMPDAB}}\text{Pd})(\text{CH}_2\text{SiMe}_3)_2$, with a focus on the role played by the activating phosphine ligand and the formation of active species in solution. By using pressurized sample infusion mass

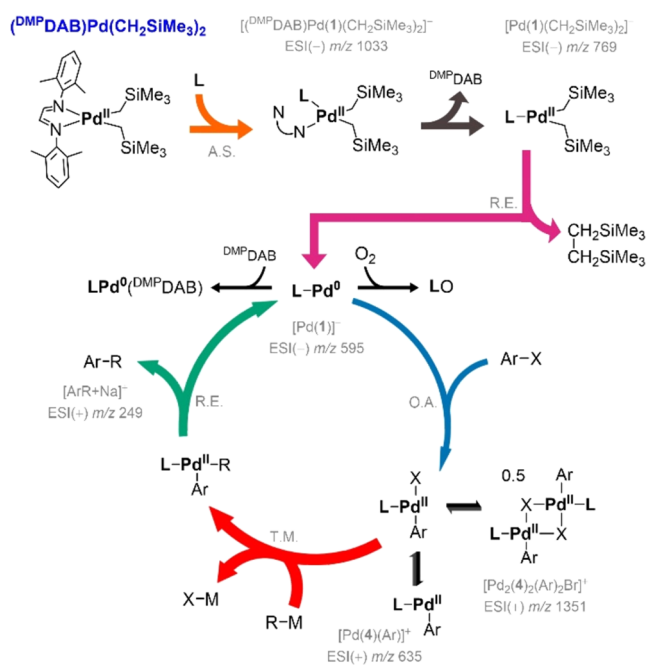


Figure 9. Proposed pathways for formation of $\text{LPd}(0)$ and $\text{LPd}(\text{II})(\text{Ar})$ species from $(^{\text{DMPDAB}}\text{Pd})(\text{CH}_2\text{SiMe}_3)_2$ precatalyst activation with diarylalkyl phosphine **1** and **4** at 1:1 Pd/L molar ratios, and oxidative addition to ArBr. Key: A.S. = associative substitution, O.A. = oxidative addition, T.M. = transmetalation, R.E. = reductive elimination; m/z ratios of key detected intermediates are shown in gray; arrow thicknesses qualitatively represent rate constants; catalytic cycle made using www.catavcycle.com.

spectrometry, this has allowed for the real-time monitoring of these processes. We demonstrate that after phosphine coordination to $(^{\text{DMPDAB}}\text{Pd})(\text{CH}_2\text{SiMe}_3)_2$, the $^{\text{DMPDAB}}$ ligand dissociates before the reductive elimination of $(\text{Me}_3\text{SiCH}_2)_2$. This sequence leads to the generation of the monoligated active catalyst $\text{LPd}(0)$. Importantly, our investigations highlight that $\text{LPd}(0)$ is the active species responsible for oxidative addition, with a considerable mechanistic barrier to bisligation favoring the formation of the highly active monoligated catalyst. We have also elucidated potential off-cycle pathways, including the possibility of competitive inhibition by $^{\text{DMPDAB}}$. All these insights will enable design of more active and robust catalyst systems for cross-coupling reactions.

EXPERIMENTAL SECTION

All experiments were setup and performed under an inert (Ar or N_2) atmosphere using standard glovebox and Schlenk line techniques.⁸³ Experiments were conducted on a Waters (Milford) Synapt G2-Si mass spectrometer and analyzed using Waters MassLynx V4.2 software. The mass spectrometer was operated in full scan resolution mode in a range of m/z 50–1500 for both negative and positive ion modes, with parameters optimized by OptiMS⁸⁶ (see SI Table S1). Calculation of theoretical m/z ratios and isotope patterns were done using PythoMS⁸⁴ and the IsoSpecPy⁸⁵ package, with identified m/z ratios summarized in the SI. Signal intensities for all chromatograms were normalized to the total ion current (TIC).

Stock solutions of $(^{\text{DMPDAB}}\text{Pd})(\text{CH}_2\text{SiMe}_3)_2$ were prepared in degassed tetrahydrofuran (THF), with all other chemical stock solutions prepared in degassed HPLC-grade methanol (MeOH). In a typical reaction, degassed HPLC-grade MeOH (10 or 20 mL) was transferred to a Schlenk flask equipped with a stirrer bar, with an aliquot of ligand and/or substrate added, and the solution sparged

with nitrogen for 15 min. The inlet system and the ESI source of the mass spectrometer were flushed with MeOH for 10 min before each experiment. The sealed flask was then connected to the spectrometer inlet via PEEK tubing (TubPEEK Red, 1/16 in. OD, 0.005 in. ID, 18 in. L). The reaction mixture was monitored by PSI-ESI-MS techniques, where an overpressure of argon gas was applied to transfer the sample solution from the Schlenk flask into the spectrometer inlet at an infusion rate of 20 $\mu\text{L min}^{-1}$. Reactions were initiated by additions of $(^{\text{DMP}}\text{DAB})\text{Pd}(\text{CH}_2\text{SiMe}_3)_2$ or substrate at specified time intervals, with the reaction allowed to proceed for up to 40 min. All reactions were stirred at 400 rpm and monitored at 60 $^\circ\text{C}$ (unless otherwise specified). Detailed experimental conditions and setup are summarized in the [Supporting Information \(SI\)](#).

■ ASSOCIATED CONTENT

SI Supporting Information

The Supporting Information is available free of charge at <https://pubs.acs.org/doi/10.1021/acs.organomet.4c00463>.

Materials and chemicals, instrument parameters, experimental procedures, and supporting investigations ([PDF](#))

■ AUTHOR INFORMATION

Corresponding Authors

David C. Leitch – Department of Chemistry, University of Victoria, Victoria, British Columbia V8W 2Y2, Canada; orcid.org/0000-0002-8726-3318; Email: dcleitch@uvic.ca

J. Scott McIndoe – Department of Chemistry, University of Victoria, Victoria, British Columbia V8W 2Y2, Canada; orcid.org/0000-0001-7073-5246; Email: mcindoe@uvic.ca

Authors

Ian C. Chagunda – Department of Chemistry, University of Victoria, Victoria, British Columbia V8W 2Y2, Canada; orcid.org/0000-0003-0578-9701

Antonia Kropp – Department of Chemistry, University of Victoria, Victoria, British Columbia V8W 2Y2, Canada

Complete contact information is available at:

<https://pubs.acs.org/doi/10.1021/acs.organomet.4c00463>

Notes

The authors declare no competing financial interest.

■ ACKNOWLEDGMENTS

I.C.C. thanks NSERC for a CGS-D award. A.K. thanks the University of Victoria for a Valerie Kuhne Undergraduate Research Award. D.C.L. thanks NSERC (Discovery, I2I) for operational funding. J.S.M. thanks the NSERC Discovery program for operational funding and NSERC RTI and the University of Victoria for infrastructural support. We thank the reviewers for their valuable input in refining this manuscript.

■ REFERENCES

- (1) Seechurn, C. C. J.; Kitching, M. O.; Colacot, T. J.; Snieckus, V. Palladium-Catalyzed Cross-Coupling: A Historical Contextual Perspective to the 2010 Nobel Prize. *Angew. Chem., Int. Ed.* **2012**, *51* (21), 5062–5085.
- (2) Gildner, P. G.; Colacot, T. J. Reactions of the 21st Century: Two Decades of Innovative Catalyst Design for Palladium-Catalyzed Cross-Couplings. *Organometallics* **2015**, *34* (23), 5497–5508.

- (3) Nicolaou, K. C.; Bulger, P. G.; Sarlah, D. Palladium-Catalyzed Cross-Coupling Reactions in Total Synthesis. *Angew. Chem., Int. Ed.* **2005**, *44* (29), 4442–4489.

- (4) Burke, A. J.; Marques, C. S.; Turner, N. J.; Hermann, G. J. Catalytic Cross-Coupling Reactions – Nobel Prize Catalysis. In *Active Pharmaceutical Ingredients in Synthesis*; John Wiley & Sons, Ltd., 2018; pp 175–257.

- (5) Campeau, L.-C.; Hazari, N. Cross-Coupling and Related Reactions: Connecting Past Success to the Development of New Reactions for the Future. *Organometallics* **2019**, *38* (1), 3–35.

- (6) Zaleskiy, S. S.; Ananikov, V. P. Pd2(Dba)3 as a Precursor of Soluble Metal Complexes and Nanoparticles: Determination of Palladium Active Species for Catalysis and Synthesis. *Organometallics* **2012**, *31* (6), 2302–2309.

- (7) Weber, P.; Biafora, A.; Doppiu, A.; Bongard, H.-J.; Kelm, H.; Gooßen, L. J. A Comparative Study of Dibenzylideneacetone Palladium Complexes in Catalysis. *Org. Process Res. Dev.* **2019**, *23* (7), 1462–1470.

- (8) Carole, W. A.; Colacot, T. J. Understanding Palladium Acetate from a User Perspective. *Chem. - Eur. J.* **2016**, *22* (23), 7686–7695.

- (9) Slack, E. D.; Tancini, P. D.; Colacot, T. J. Process Economics and Atom Economy for Industrial Cross Coupling Applications via LnPd(0)-Based Catalysts. In *Organometallics in Process Chemistry*; Colacot, T. J.; Sivakumar, V., Eds.; Springer International Publishing: Cham, 2019; pp 161–198.

- (10) Ting, M. Y. C.; Yunker, L. P. E.; Chagunda, I. C.; Hatlelid, K.; Vieweg, M.; McIndoe, J. S. A Mechanistic Investigation of the Suzuki Polycondensation Reaction Using MS/MS Methods. *Catal. Sci. Technol.* **2021**, *11* (13), 4406–4416.

- (11) Firsan, S. J.; Sivakumar, V.; Colacot, T. J. Emerging Trends in Cross-Coupling: Twelve-Electron-Based L1Pd(0) Catalysts, Their Mechanism of Action, and Selected Applications. *Chem. Rev.* **2022**, *122* (23), 16983–17027.

- (12) Lau, S. H.; Chen, L.; Kevlishvili, I.; Davis, K.; Liu, P.; Carrow, B. Capturing the Most Active State of a Palladium(0) Cross-Coupling Catalyst *ChemRxiv* 2021 DOI: [10.26434/chemrxiv-2021-477kn](https://doi.org/10.26434/chemrxiv-2021-477kn).

- (13) Semeniuchenko, V.; Sharif, S.; Rana, N.; Chandrasoma, N.; Braje, W. M.; Baker, R. T.; Manthorpe, J. M.; Pietro, W. J.; Organ, M. G. Experimental Evidence for Zerovalent Pd(NHC) as a Competent Catalyst in C–N Cross-Coupling (NHC = DiMeIHeptCl). *J. Am. Chem. Soc.* **2024**, *146* (42), 29224–29236.

- (14) MacQueen, P. M.; Holley, R.; Ghorai, S.; Colacot, T. J. Convenient One-Pot Synthesis of L2Pd(0) Complexes for Cross-Coupling Catalysis. *Organometallics* **2023**, *42* (18), 2644–2650.

- (15) Li, H.; Seechurn, C. C. C. J.; Colacot, T. J. Development of Preformed Pd Catalysts for Cross-Coupling Reactions, Beyond the 2010 Nobel Prize. *ACS Catal.* **2012**, *2* (6), 1147–1164.

- (16) Vikse, K.; Naka, T.; McIndoe, J. S.; Besora, M.; Maseras, F. Oxidative Additions of Aryl Halides to Palladium Proceed through the Monoligated Complex. *ChemCatChem* **2013**, *5* (12), 3604–3609.

- (17) Scharf, L. T.; Rodstein, I.; Schmidt, M.; Scherpf, T.; Gessner, V. H. Unraveling the High Activity of Ylide-Functionalized Phosphines in Palladium-Catalyzed Amination Reactions: A Comparative Study with CyJohnPhos and PtBu3. *ACS Catal.* **2020**, *10* (2), 999–1009.

- (18) Newman-Stonebraker, S. H.; Smith, S. R.; Borowski, J. E.; Peters, E.; Gensch, T.; Johnson, H. C.; Sigman, M. S.; Doyle, A. G. Univariate Classification of Phosphine Ligation State and Reactivity in Cross-Coupling Catalysis. *Science* **2021**, *374* (6565), 301–308.

- (19) Scott, N. W. J.; Ford, M. J.; Jeddi, N.; Eyles, A.; Simon, L.; Whitwood, A. C.; Tanner, T.; Willans, C. E.; Fairlamb, I. J. S. A Dichotomy in Cross-Coupling Site Selectivity in a Dihalogenated Heteroarene: Influence of Mononuclear Pd, Pd Clusters, and Pd Nanoparticles—the Case for Exploiting Pd Catalyst Speciation. *J. Am. Chem. Soc.* **2021**, *143* (25), 9682–9693.

- (20) Niemeyer, Z. L.; Milo, A.; Hickey, D. P.; Sigman, M. S. Parameterization of Phosphine Ligands Reveals Mechanistic Pathways and Predicts Reaction Outcomes. *Nat. Chem.* **2016**, *8* (6), 610–617.

- (21) Besora, M.; Maseras, F. The Diverse Mechanisms for the Oxidative Addition of C–Br Bonds to Pd(PR3) and Pd(PR3)2 Complexes. *Dalton Trans.* **2019**, *48* (43), 16242–16248.
- (22) Norman, J. P.; Larson, N. G.; Neufeldt, S. R. Different Oxidative Addition Mechanisms for 12- and 14-Electron Palladium(0) Explain Ligand-Controlled Divergent Site Selectivity. *ACS Catal.* **2022**, *12* (15), 8822–8828.
- (23) Kania, M. J.; Reyes, A.; Neufeldt, S. R. Oxidative Addition of (Hetero)Aryl (Pseudo)Halides at Palladium(0): Origin and Significance of Divergent Mechanisms. *J. Am. Chem. Soc.* **2024**, *146* (28), 19249–19260.
- (24) Marion, N.; Navarro, O.; Mei, J.; Stevens, E. D.; Scott, N. M.; Nolan, S. P. Modified (NHC)Pd(Allyl)Cl (NHC = N-Heterocyclic Carbene) Complexes for Room-Temperature Suzuki–Miyaura and Buchwald–Hartwig Reactions. *J. Am. Chem. Soc.* **2006**, *128* (12), 4101–4111.
- (25) Seechurn, C. C. C. J.; Parisel, S. L.; Colacot, T. J. Air-Stable Pd(R-Allyl)LCl (L = Q-Phos, P(t-Bu)₃, Etc.) Systems for C–C/N Couplings: Insight into the Structure–Activity Relationship and Catalyst Activation Pathway. *J. Org. Chem.* **2011**, *76* (19), 7918–7932.
- (26) Hill, L. L.; Crowell, J. L.; Tutwiler, S. L.; Massie, N. L.; Hines, C. C.; Griffin, S. T.; Rogers, R. D.; Shaughnessy, K. H.; Grasa, G. A.; Seechurn, C. C. C. J.; Li, H.; Colacot, T. J.; Chou, J.; Woltermann, C. J. Synthesis and X-Ray Structure Determination of Highly Active Pd(II), Pd(I), and Pd(0) Complexes of Di(Tert-Butyl)-Neopentylphosphine (DTBNpP) in the Arylation of Amines and Ketones. *J. Org. Chem.* **2010**, *75* (19), 6477–6488.
- (27) Melvin, P. R.; Nova, A.; Balcells, D.; Dai, W.; Hazari, N.; Hruszkewycz, D. P.; Shah, H. P.; Tudge, M. T. Design of a Versatile and Improved Precatalyst Scaffold for Palladium-Catalyzed Cross-Coupling: (H3–1-tBu-Indenyl)2(μ-Cl)2Pd2. *ACS Catal.* **2015**, *5* (6), 3680–3688.
- (28) Ingoglia, B. T.; Buchwald, S. L. Oxidative Addition Complexes as Precatalysts for Cross-Coupling Reactions Requiring Extremely Bulky Biarylphosphine Ligands. *Org. Lett.* **2017**, *19* (11), 2853–2856.
- (29) Biscoe, M. R.; Fors, B. P.; Buchwald, S. L. A New Class of Easily Activated Palladium Precatalysts for Facile C–N Cross-Coupling Reactions and the Low Temperature Oxidative Addition of Aryl Chlorides. *J. Am. Chem. Soc.* **2008**, *130* (21), 6686–6687.
- (30) Bruno, N. C.; Tudge, M. T.; Buchwald, S. L. Design and Preparation of New Palladium Precatalysts for C–C and C–N Cross-Coupling Reactions. *Chem. Sci.* **2013**, *4* (3), 916–920.
- (31) Barnett, K. L.; Howard, J. R.; Treager, C. J.; Shipley, A. T.; Stullich, R. M.; Qu, F.; Gerlach, D. L.; Shaughnessy, K. H. Air-Stable [(R3P)PdCl2]2 Complexes of Neopentylphosphines as Cross-Coupling Precatalysts: Catalytic Application and Mechanism of Catalyst Activation and Deactivation. *Organometallics* **2018**, *37* (9), 1410–1424.
- (32) Nasielski, J.; Hadei, N.; Achonduh, G.; Kantchev, E. A. B.; O'Brien, C. J.; Lough, A.; Organ, M. G. Structure–Activity Relationship Analysis of Pd–PEPPSI Complexes in Cross-Couplings: A Close Inspection of the Catalytic Cycle and the Precatalyst Activation Model. *Chem. - Eur. J.* **2010**, *16* (35), 10844–10853.
- (33) Durà-Vilà, V.; Mingos, D. M. P.; Vilar, R.; White, A. J. P.; Williams, D. J. Reactivity Studies of [Pd2(μ-X)2(PBu3)2] (X = Br, I) with CNR (R = 2,6-Dimethylphenyl), H2 and Alkynes. *J. Organomet. Chem.* **2000**, *600* (1), 198–205.
- (34) Carole, W.; Colacot, T.; Seechurn, C.; Scrase, T. WO Patent, WO2018073559, 2018. <https://patentscope.wipo.int/search/en/detail.jsf?docId=WO2018073559>.
- (35) Auffero, M.; Scattolin, T.; Proutière, F.; Schoenebeck, F. Air-Stable Dinuclear Iodine-Bridged Pd(I) Complex - Catalyst, Precursor, or Parasite? The Additive Decides. Systematic Nucleophile-Activity Study and Application as Precatalyst in Cross-Coupling. *Organometallics* **2015**, *34* (20), 5191–5195.
- (36) Schmid, T. E.; Jones, D. C.; Songis, O.; Diebolt, O.; Furst, M. R. L.; Slawin, A. M. Z.; Cazin, C. S. J. Mixed Phosphine/N-Heterocyclic Carbene Palladium Complexes: Synthesis, Characterization and Catalytic Use in Aqueous Suzuki–Miyaura Reactions. *Dalton Trans.* **2013**, *42* (20), 7345–7353.
- (37) Shaughnessy, K. H. Development of Palladium Precatalysts That Efficiently Generate LPd(0) Active Species. *Isr. J. Chem.* **2020**, *60* (3–4), 180–194.
- (38) Andreu, M. G.; Zapf, A.; Beller, M. Molecularly Defined Palladium(0) Monophosphine Complexes as Catalysts for Efficient Cross-Coupling of Aryl Chlorides and Phenylboronic Acid1. *Chem. Commun.* **2000**, *24*, 2475–2476.
- (39) Tschan, M. J.-L.; García-Suárez, E. J.; Freixa, Z.; Launay, H.; Hagen, H.; Benet-Buchholz, J.; van Leeuwen, P. W. N. M. Efficient Bulky Phosphines for the Selective Telomerization of 1,3-Butadiene with Methanol. *J. Am. Chem. Soc.* **2010**, *132* (18), 6463–6473.
- (40) Lee, H. G.; Milner, P. J.; Buchwald, S. L. An Improved Catalyst System for the Pd-Catalyzed Fluorination of (Hetero)Aryl Triflates. *Org. Lett.* **2013**, *15* (21), 5602–5605.
- (41) Lee, H. G.; Milner, P. J.; Colvin, M. T.; Andreas, L.; Buchwald, S. L. Structure and Reactivity of [(L-Pd)*n*-(1,5-Cyclooctadiene)] (*n* = 1–2) Complexes Bearing Biaryl Phosphine Ligands. *Inorg. Chim. Acta* **2014**, *422*, 188–192.
- (42) Huang, J.; Isaac, M.; Watt, R.; Becica, J.; Dennis, E.; Saidaminov, M. I.; Sabbers, W. A.; Leitch, D. C. DMPDAB–Pd–MAH: A Versatile Pd(0) Source for Precatalyst Formation, Reaction Screening, and Preparative-Scale Synthesis. *ACS Catal.* **2021**, *11* (9), 5636–5646.
- (43) Bigler, R.; Spiess, D.; Wellauer, J.; Binder, M.; Carré, V.; Fantasia, S. Synthesis of Biaryl Phosphine Palladium(0) Precatalysts. *Organometallics* **2021**, *40* (15), 2384–2388.
- (44) Huang, J.; Ho, D. B.; Gaube, G.; Celuszak, H.; Becica, J.; Thomas, G. T.; Schley, N. D.; Leitch, D. C. A Thermally Stable, Alkene-Free Palladium Source for Oxidative Addition Complex Formation and High-Turnover Catalysis. *Organometallics* **2024**, *43* (20), 2403–2412.
- (45) Uehling, M. R.; King, R. P.; Krska, S. W.; Cernak, T.; Buchwald, S. L. Pharmaceutical Diversification via Palladium Oxidative Addition Complexes. *Science* **2019**, *363* (6425), 405–408.
- (46) Chagunda, I. C.; Kropp, A.; Leitch, D. C.; McIndoe, J. S. Ligand Substitution, Catalyst Activation, and Oxidative Addition Studies of a Stable Dialkyl Palladium Precatalyst *ChemRxiv* 2024 DOI: 10.26434/chemrxiv-2024-nx480.
- (47) Thomas, G. T.; Donneck, S.; Chagunda, I. C.; McIndoe, J. S. Pressurized Sample Infusion. *Chem.: Methods* **2022**, *2* (1), No. e202100068.
- (48) McMullin, C. L.; Fey, N.; Harvey, J. N. Computed Ligand Effects on the Oxidative Addition of Phenyl Halides to Phosphine Supported Palladium(0) Catalysts. *Dalton Trans.* **2014**, *43* (36), 13545–13556.
- (49) Vidossich, P.; Ujaque, G.; Lledós, A. Palladium Monophosphine Pd(PPh₃): Is It Really Accessible in Solution? *Chem. Commun.* **2014**, *50* (6), 661–663.
- (50) Ahlquist, M.; Fristrup, P.; Tanner, D.; Norrby, P.-O. Theoretical Evidence for Low-Ligated Palladium(0): [Pd–L] as the Active Species in Oxidative Addition Reactions. *Organometallics* **2006**, *25* (8), 2066–2073.
- (51) Li, Z.; Fu, Y.; Guo, Q.-X.; Liu, L. Theoretical Study on Monoligated Pd-Catalyzed Cross-Coupling Reactions of Aryl Chlorides and Bromides. *Organometallics* **2008**, *27* (16), 4043–4049.
- (52) Zheng, Q.; Liu, Y.; Chen, Q.; Hu, M.; Helmy, R.; Sherer, E. C.; Welch, C. J.; Chen, H. Capture of Reactive Monophosphine-Ligated Palladium(0) Intermediates by Mass Spectrometry. *J. Am. Chem. Soc.* **2015**, *137* (44), 14035–14038.
- (53) Chagunda, I. C.; Williams, P. J. H.; Fisher, T.; Stock, N. L.; Beach, D. G.; Thomas, G. T.; Zhu, J.; McIndoe, J. S. Comparative Assessment of ESI-MS Softness for Inorganic Complexes: How Soft Is Your ESI-MS? *Eur. J. Inorg. Chem.* **2024**, *27*, No. e202400077.
- (54) Schröder, D. Applications of Electrospray Ionization Mass Spectrometry in Mechanistic Studies and Catalysis Research. *Acc. Chem. Res.* **2012**, *45* (9), 1521–1532.

- (55) McDonald, L. W. I.; Campbell, J. A.; Clark, S. B. Failure of ESI Spectra to Represent Metal-Complex Solution Composition: A Study of Lanthanide–Carboxylate Complexes. *Anal. Chem.* **2014**, *86* (2), 1023–1029.
- (56) Williams, P. J. H.; Chagunda, I. C.; McIndoe, J. S. OptiMS: An Accessible Program for Automating Mass Spectrometry Parameter Optimization and Configuration. *J. Am. Soc. Mass Spectrom.* **2024**, *35* (3), 449–455.
- (57) Thomas, G. T.; Janusson, E.; Zijlstra, H. S.; McIndoe, J. S. Step-by-Step Real Time Monitoring of a Catalytic Amination Reaction. *Chem. Commun.* **2019**, *55* (78), 11727–11730.
- (58) Yunker, L. P. E.; Ahmadi, Z.; Logan, J. R.; Wu, W.; Li, T.; Martindale, A.; Oliver, A. G.; McIndoe, J. S. Real-Time Mass Spectrometric Investigations into the Mechanism of the Suzuki–Miyaura Reaction. *Organometallics* **2018**, *37* (22), 4297–4308.
- (59) Tereniak, S. J.; Landis, C. R.; Stahl, S. S. Are Phosphines Viable Ligands for Pd-Catalyzed Aerobic Oxidation Reactions? Contrasting Insights from a Survey of Six Reactions. *ACS Catal.* **2018**, *8* (4), 3708–3714.
- (60) Barder, T. E.; Buchwald, S. L. Insights into Amine Binding to Biaryl Phosphine Palladium Oxidative Addition Complexes and Reductive Elimination from Biaryl Phosphine Arylpalladium Amido Complexes via Density Functional Theory. *J. Am. Chem. Soc.* **2007**, *129* (39), 12003–12010.
- (61) Arrechea, P. L.; Buchwald, S. L. Biaryl Phosphine Based Pd(II) Amido Complexes: The Effect of Ligand Structure on Reductive Elimination. *J. Am. Chem. Soc.* **2016**, *138* (38), 12486–12493.
- (62) Newman-Stonebraker, S. H.; Wang, J. Y.; Jeffrey, P. D.; Doyle, A. G. Structure–Reactivity Relationships of Buchwald-Type Phosphines in Nickel-Catalyzed Cross-Couplings. *J. Am. Chem. Soc.* **2022**, *144* (42), 19635–19648.
- (63) Milstein, D.; Stille, J. K. Mechanism of Reductive Elimination. Reaction of Alkylpalladium(II) Complexes with Tetraorganotin, Organolithium, and Grignard Reagents. Evidence for Palladium(IV) Intermediacy. *J. Am. Chem. Soc.* **1979**, *101* (17), 4981–4991.
- (64) Gillie, A.; Stille, J. K. Mechanisms of 1,1-Reductive Elimination from Palladium. *J. Am. Chem. Soc.* **1980**, *102* (15), 4933–4941.
- (65) Tatsumi, K.; Hoffmann, R.; Yamamoto, A.; Stille, J. K. Reductive Elimination of D8-Organotransition Metal Complexes. *Bull. Chem. Soc. Jpn.* **1981**, *54* (6), 1857–1867.
- (66) Komiya, S.; Albright, T. A.; Hoffmann, R.; Kochi, J. K. Reductive Elimination and Isomerization of Organogold Complexes. Theoretical Studies of Trialkylgold Species as Reactive Intermediates. *J. Am. Chem. Soc.* **1976**, *98* (23), 7255–7265.
- (67) Pérez-Rodríguez, M.; Braga, A. A. C.; de Lera, A. R.; Maseras, F.; Álvarez, R.; Espinet, P. A DFT Study of the Effect of the Ligands in the Reductive Elimination from Palladium Bis(Allyl) Complexes. *Organometallics* **2010**, *29* (21), 4983–4991.
- (68) Christmann, U.; Vilar, R. Monoligated Palladium Species as Catalysts in Cross-Coupling Reactions. *Angew. Chem., Int. Ed.* **2005**, *44* (3), 366–374.
- (69) Schoenebeck, F.; Houk, K. N. Ligand-Controlled Regioselectivity in Palladium-Catalyzed Cross Coupling Reactions. *J. Am. Chem. Soc.* **2010**, *132* (8), 2496–2497.
- (70) Barder, T. E.; Biscoe, M. R.; Buchwald, S. L. Structural Insights into Active Catalyst Structures and Oxidative Addition to (Biaryl)-phosphine–Palladium Complexes via Density Functional Theory and Experimental Studies. *Organometallics* **2007**, *26* (9), 2183–2192.
- (71) Martin, R.; Buchwald, S. L. Palladium-Catalyzed Suzuki–Miyaura Cross-Coupling Reactions Employing Dialkylbiaryl Phosphine Ligands. *Acc. Chem. Res.* **2008**, *41* (11), 1461–1473.
- (72) Yadav, M. R.; Nagaoka, M.; Kashihara, M.; Zhong, R.-L.; Miyazaki, T.; Sakaki, S.; Nakao, Y. The Suzuki–Miyaura Coupling of Nitroarenes. *J. Am. Chem. Soc.* **2017**, *139* (28), 9423–9426.
- (73) Janusson, E.; Zijlstra, H. S.; Nguyen, P. P. T.; MacGillivray, L.; Martelino, J.; McIndoe, J. S. Real-Time Analysis of Pd2(Dba)3 Activation by Phosphine Ligands. *Chem. Commun.* **2017**, *53* (5), 854–856.
- (74) Chagunda, I. C.; Fisher, T.; Schierling, M.; McIndoe, J. S. Poisonous Truth about the Mercury Drop Test: The Effect of Elemental Mercury on Pd(0) and Pd(II)ArX Intermediates. *Organometallics* **2023**, *42* (19), 2938–2945.
- (75) Henderson, W.; Evans, C. Electrospray Mass Spectrometric Analysis of Transition-Metal Halide Complexes. *Inorg. Chim. Acta* **1999**, *294* (2), 183–192.
- (76) Santos, L. S.; Rosso, G. B.; Pilli, R. A.; Eberlin, M. N. The Mechanism of the Stille Reaction Investigated by Electrospray Ionization Mass Spectrometry. *J. Org. Chem.* **2007**, *72* (15), 5809–5812.
- (77) Brazier, J. B.; Newton, M. A.; Barreiro, E. M.; Adrio, L. A.; Naya, L.; Hii, K. K. M. Solvent-Dependent Nuclearity, Geometry and Catalytic Activity of [(SPhos)Pd(Ph)Cl]2. *Dalton Trans.* **2017**, *46* (22), 7223–7231.
- (78) Agrawal, D.; Zins, E.-L.; Schröder, D. Intramolecular Scrambling of Aryl Groups in Organopalladium Complexes [ArPd-(PPh3)2]+: From Solution to the Gas Phase, Back Again, and In-Between. *Chem. - Asian J.* **2010**, *5* (7), 1667–1676.
- (79) Morita, D. K.; Stille, J. K.; Norton, J. R. Methyl/Phenyl Exchange between Palladium and a Phosphine Ligand. Consequences for Catalytic Coupling Reactions. *J. Am. Chem. Soc.* **1995**, *117* (33), 8576–8581.
- (80) Fiebig, L.; Schlörer, N.; Schmalz, H.-G.; Schäfer, M. Aryl–Phenyl Scrambling in Intermediate Organopalladium Complexes: A Gas-Phase Study of the Mizoroki–Heck Reaction. *Chem. - Eur. J.* **2014**, *20* (17), 4906–4910.
- (81) Lee, Y. H.; Morandi, B. Transition Metal-Mediated Metathesis between P–C and M–C Bonds: Beyond a Side Reaction. *Coord. Chem. Rev.* **2019**, *386*, 96–118.
- (82) McFarlane, J.; Henderson, B.; Donnecke, S.; McIndoe, J. S. An Information-Rich Graphical Representation of Catalytic Cycles. *Organometallics* **2019**, *38* (21), 4051–4053.
- (83) Borys, A. M. An Illustrated Guide to Schlenk Line Techniques. *Organometallics* **2023**, *42* (3), 182–196.
- (84) Yunker, L. P. E.; Donnecke, S.; Ting, M.; Yeung, D.; McIndoe, J. S. PythoMS: A Python Framework To Simplify and Assist in the Processing and Interpretation of Mass Spectrometric Data. *J. Chem. Inf. Model.* **2019**, *59* (4), 1295–1300.
- (85) Łącki, M. K.; Startek, M.; Valkenborg, D.; Gambin, A. IsoSpec: Hyperfast Fine Structure Calculator. *Anal. Chem.* **2017**, *89* (6), 3272–3277.